Coexisting Stripe- and Patch-Shaped Domains in Giant Unilamellar Vesicles†

Li Li and Ji-Xin Cheng*

Weldon School of Biomedical Engineering and Department of Chemistry, Purdue University, West Lafayette, Indiana 47907

Received April 25, 2006; Revised Manuscript Received July 25, 2006

ABSTRACT: We report a new type of gel−liquid phase segregation in giant unilamellar vesicles (GUVs) of mixed lipids. Coexisting patch- and stripe-shaped gel domains in GUV bilayers composed of DOPC/DPPC or DLPC/DPPC are observed by confocal fluorescence microscopy. The lipids in stripe domains are shown to be tilted according to the DiIC18 fluorescence intensity dependence on the excitation polarization. The patch domains are found to be mainly composed of DPPC-d_{62} according to the coherent anti-Stokes Raman scattering (CARS) images of DOPC/DPPC-d_{62} bilayers. When cooling GUVs from above the miscibility temperature, the patch domains start to appear between the chain melting and the pretransition temperature of DPPC. In GUVs containing a high molar percentage of DPPC, the stripe domains form below the pretransition temperature. Our observations suggest that the patch and stripe domains are in the $P_{\beta'}$ and $L_{\beta'}$ gel phases, respectively. According to the thermoelastic properties of GUVs described by Needham and Evans [(1988) *Biochemistry 27*, 8261−8269], the $P_{\beta'}$ and $L_{\beta'}$ phases are formed at relatively low and high membrane tensions, respectively. GUVs with high DPPC percentage have high membrane surface tension and thus mainly exhibit $L_{\beta'}$ domains, while GUVs with low DPPC percentage have low membrane surface tension and form $P_{\beta'}$ domains accordingly. Adding negatively charged lipid to the lipid mixtures or applying an osmotic pressure to GUVs using sucrose solutions releases the surface tension and leads to the disappearance of the $L_{\beta'}$ gel phase. The relationship between the observed domains in free-standing GUV bilayers and those in supported bilayers is discussed.

Phase segregation plays important roles in membrane organization and intracellular trafficking (*1*−*5*). The phase behavior of lipid mixtures has been extensively studied using different well-defined model membrane systems. GUVs[1] which mimic the plasma membrane with controlled lipid compositions and similar size as cells have been widely used to study the mechanisms of membrane phase segregation, fusion, and fission (*6*−*10*). In GUVs composed of a saturated lipid, an unsaturated lipid, and cholesterol, the observation of coexisting ordered and disordered liquid phases below the miscibility transition temperature has provided supports for the existence of lipid rafts in cell membranes (*11*). Despite these advances, the lipid phase behavior in GUVs is far away from being well understood, even for binary lipid mixtures. Patch- and stripe-shaped domains in GUVs composed of DPPC and another phospholipid have been reported in different papers (*7*, *8*, *12*, *13*). However, the composition and lipid organization properties of these domains have not been well characterized. The relations between these two types of domains and the different gel phases ($P_{\beta'}$ and $L_{\beta'}$) observed in pure DPPC bilayers are elusive. In addition, the forces that govern the formation of these two types of domains are poorly investigated.

In this paper, we address the above issues through a systematic imaging study of phase segregation in GUV bilayers composed of DPPC/DOPC or DPPC/DLPC. Using confocal fluorescence microscopy, we observed coexisting stripe- and patch-shaped domains in both types of GUVs at certain composition ranges. The stripe domains can be labeled by Rh-DPPE or DiIC18. The excitation polarization dependence of the fluorescence from DiIC18 shows the tilting of lipids in the stripe domains. The patch domains cannot be labeled by fluorescent probes. Our CARS images show that the patch domains are enriched in DPPC-d_{62}. In a temperature-controlled chamber, the patch domains start to appear when the GUVs are cooled to a temperature between the chain melting and the pretransition temperature of DPPC. Further cooling causes the growth of stripe domains starting from the patch domain sites. Reducing the membrane tension by adding negatively charged lipid into the lipid mixtures or growing GUVs in sucrose solutions eliminates the formation of stripe domains. On the basis of these characterizations and the thermoelastic properties of GUVs described by Needham and Evans (*14*), we propose that the stripe and patch domains are in the $L_{\beta'}$ and $P_{\beta'}$ phases, respectively.

MATERIALS AND METHODS

Lipids. DOPC, DPPC, DLPC, DPPC-d_{62}, Rh-DPPE, DOPG, and Rh-DOPE were purchased from Avanti Polar

† This work is supported by NSF Grant 0416785 and NIH R21 Grant EB004966-01.

* To whom correspondence should be addressed. Telephone: 765-494-4335. Fax: 765-494-1193. E-mail: jcheng@purdue.edu.

[1] Abbreviations: DOPC, dioleoylphosphatidylcholine; DLPC, dilauroylphosphatidylcholine; DPPC, dipalmitoylphosphatidylcholine; DOPG, dioleoylphosphatidylglycerol; DPPC-d_{62}, DPPC with fully deuterated acyl chains; Rh-DPPE, 1,2-dipalmitoyl-*sn*-glycero-3-phosphoethanolamine-*N*-(lissamine rhodamine B sulfonyl); Rh-DOPE, 1,2-dioleoyl-*sn*-glycero-3-phosphoethanolamine-*N*-(lissamine rhodamine B sulfonyl); BODIPY PC, 2-(4,4-difluoro-5,7-dimethyl-4-bora-3a,4a-diaza-*s*-indacene-3-pentanoyl)-1-hexadecanoyl-*sn*-glycero-3-phosphocholine; DiIC18, 1,1′-dioctadecyl-3,3,3′,3′-tetramethylindodicarbocyanine, 4-chlorobenzenesulfonate salt; CARS, coherent anti-Stokes Raman scattering; GUV, giant unilamellar vesicle.

10.1021/bi060808h CCC: $33.50
Published on Web 09/07/2006

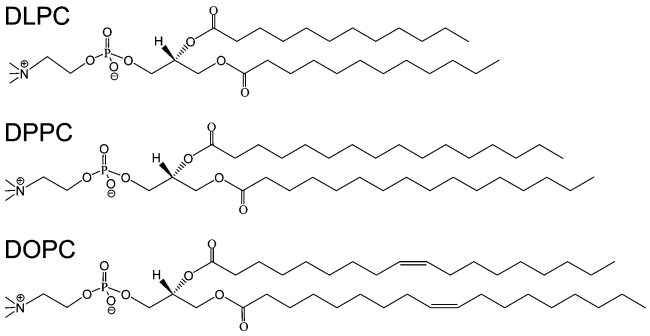

FIGURE 1: Molecular structure of DLPC, DPPC, and DOPC.

Lipids (Alabaster, AL) and used without further purification. DiIC18 and BODIPY PC were purchased from Molecular Probes (Eugene, OR). The molecular structures of DOPC, DPPC, and DLPC are shown in Figure 1.

Preparation of GUVs and Planar Bilayers. Giant unilamellar vesicles are prepared using the electroformation method (*15*). The total concentration of the lipid mixtures in a chloroform solution is 0.2 μmol/mL, containing 0.4 mol % BODIPY PC and 0.4 mol % Rh-DPPE. A 10 μL glass syringe is used to add 10 μL of the mixture solution evenly onto the conducting side of an indium tin oxide (ITO) coated glass slide. After 1 h under vacuum, the electroformation cell composed of the ITO coverglass and a poly(dimethylsiloxane) spacer is filled with milli-Q water and then sealed with a second ITO glass with the conductive side facing the water. Electroformation is carried out by using a 10 Hz sine wave with a $V_{peak-peak}$ of 2.4 V for 2 h at 50 °C. The samples are cooled to room temperature (23 °C) at a rate of 0.13 deg/min.

Confocal Fluorescence Imaging. Confocal fluorescence images of GUVs are acquired with an inverted microscope (Olympus, FV300/IX70) equipped with a 40× water immersion objective (Olympus, 1-UM568, working distance 3.3 mm). A 488 nm Ar^+ laser and a 543 nm HeNe laser are simultaneously used to excite BODIPY PC and Rh-DPPE (or DiIC18), respectively. A half wave plate is used to control the 543 nm beam polarization direction. For temperature dependence studies the electroformation cell is placed in a home-built temperature-controlled chamber.

Laser-Scanning CARS Imaging. A schematic of our CARS microscope is shown elsewhere (*16*). Briefly, two collinearly combined 2.5 ps pulse trains at frequencies ω_p and ω_s are generated from two synchronized Ti:sapphire oscillators (Coherent Inc., Mira 900). A Pockels' cell (Conoptics, no. 350-160) is used to lower the repetition rate to 3.8 MHz. CARS images are acquired by raster scanning the two laser beams using the same confocal microscope. A 60× water immersion objective with 1.2 numerical aperture is used to focus the laser beams into the sample. The backward CARS signal is collected by the same water objective and detected by a photomultiplier tube (Hamamatsu, H7422-40) with quantum efficiency of 0.4 at the CARS wavelength around 600 nm.

RESULTS

Room temperature confocal fluorescence images of GUVs composed of DPPC/DOPC at increasing molar percentage of DPPC are shown in Figure 2. GUVs are labeled by 0.4 mol % BODIPY PC and Rh-DPPE. Each image is an overlay of two simultaneously acquired fluorescence signals from BODIPY PC (pseudo color green) and Rh-DPPE (pseudo color red). In GUVs containing 10% or 20% DPPC, the fluorescent probes BODIPY PC (green) and Rh-DPPE (red) are uniformly distributed in the GUV bilayer (Figure 2A,B). Increasing the DPPC molar fraction results in visible liquid−gel phase segregation. With 30%, 40%, or 50% DPPC the GUVs segregate into patch domains and the continuous liquid phase labeled by BODIPY PC and Rh-DPPE (Figure 2C−E). The patch domains appear dark due to little partition of either BODIPY PC or Rh-DPPE. The domain shapes can be hexagonal, rhombic, six-cornered star, dumbbell, or dendritic as described by Bagatolli et al. (*8*). The overall patch domain area on GUV surface increases with increasing DPPC molar percentage. With 60% DPPC we observed another type of domain that has a stripe shape and coexists with the patch domain (see Figure 2F). Rh-DPPE preferentially partitions into the stripe domains, consistent with previous observation by Bagatolli (*8*). With the DPPC molar fraction increased to 80%, the stripe domains become wider and form a network while the patch domain area shrinks (Figure 2G,H). For GUVs containing 90% DPPC, patch domains nearly vanish and the network-forming stripe domains dominate the whole GUV surface (see Figure 2I). For each composition, the image represents the major GUV population in the electroformation chamber. To ensure that the observed domains are not induced by probes, we have tried different molar concentrations (0.01%, 0.1%, and 1.0%) of Rh-DPPE and BODIPY PC (data not shown). The domain pattern was found to be independent of the probe concentrations over the range tested. We also used DiIC18 to label the stripe domains and Rh-DOPE to label the liquid phase separately. The same domain pattern has been observed (data not shown).

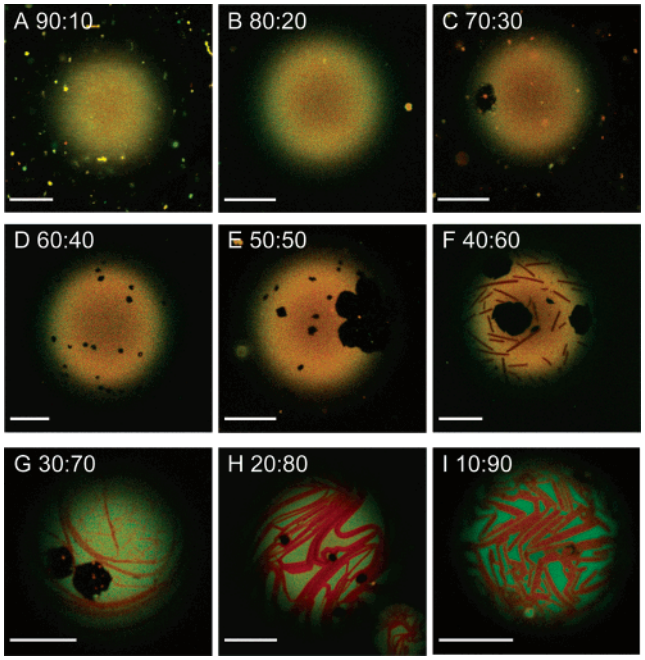

FIGURE 2: Confocal fluorescence images of GUVs composed of DOPC and DPPC at different molar ratios. The ratio of DOPC:DPPC is marked in each image. Each image is an overlay of two simultaneously acquired fluorescence signals from BODIPY PC (pseudo color green) and Rh-DPPE (pseudo color red). The laser beams were focused onto the top part of the GUVs. All of the images were taken at room temperature (23 °C). Bar = 10 μm.

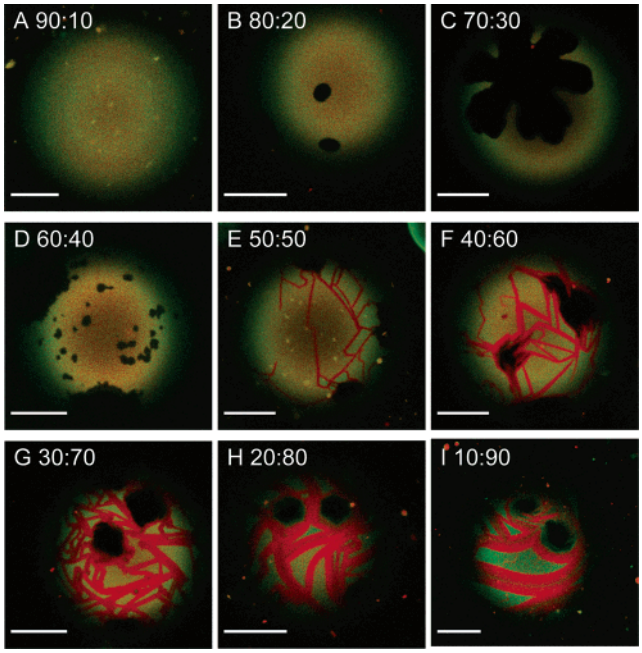

FIGURE 3: Confocal fluorescence images of GUVs composed of DLPC and DPPC at different molar ratios. The ratio of DLPC:DPPC is marked in each image. Each image is an overlay of two simultaneously acquired fluorescence signals from BODIPY PC (pseudo color green) and Rh-DPPE (pseudo color red). The acquisition conditions are the same as in Figure 2. Bar = 10 μm.

The phase segregation in DOPC/DPPC GUVs is induced by the mismatch between unsaturated and saturated hydrocarbon chains. To find out whether the coexistence of patch and stripe domains can occur to GUVs composed of DPPC and a saturated phosphocholine, we studied GUVs of DLPC/DPPC at different molar ratios. The same amount of BODIPY PC and Rh-DPPE as used in the DOPC/DPPC system was added into the lipid mixture. The melting temperature (T_m) of DLPC and DPPC is -1 and 42 °C, respectively, as a result of different acyl chain lengths (Figure 1). At room temperature (23 °C), we clearly observed analogous coexisting patch- and stripe-shaped domains in GUVs over a range of compositions (Figure 3). However, the coexistence region is expanded compared to the case of DOPC/DPPC. The patch/stripe domain coexistence is observed from 60% to 80% DPPC in GUVs of DOPC/DPPC, while from 50% to 90% DPPC in GUVs of DLPC/DPPC.

The stripe-shaped domains have been observed in GUVs of DOPC/DPPC (*12*), DLPC/DPPC (*8*), and POPC/DPPC (*13*). To determine the lipid chain orientation in the stripe domains, we utilized polarized fluorescence microscopy which has been used for probing the molecular orientation in NBD-DPPE-labeled monolayers (*17*). We have studied the stripe domains in DLPC/DPPC GUVs labeled by DiIC18 using polarized light excitation. We first characterized the dipole orientation in DiIC18 using a liquid-phase GUV composed of 9:1 DLPC/DPPC. With the laser beam focused on the equatorial plane of the liquid-phase GUV (Figure 4A,B), the DiIC18 fluorescence intensity is maximized and minimized when the bilayer normal is parallel with and perpendicular to the excitation polarization, respectively. This indicates that the electronic absorption dipole of DiIC18 is oriented along the bilayer chains as shown in Figure 4C. For a stripe domain extending along the *y* direction at the top of a GUV composed of 1:9 DLPC/DPPC (Figure 4D,E),

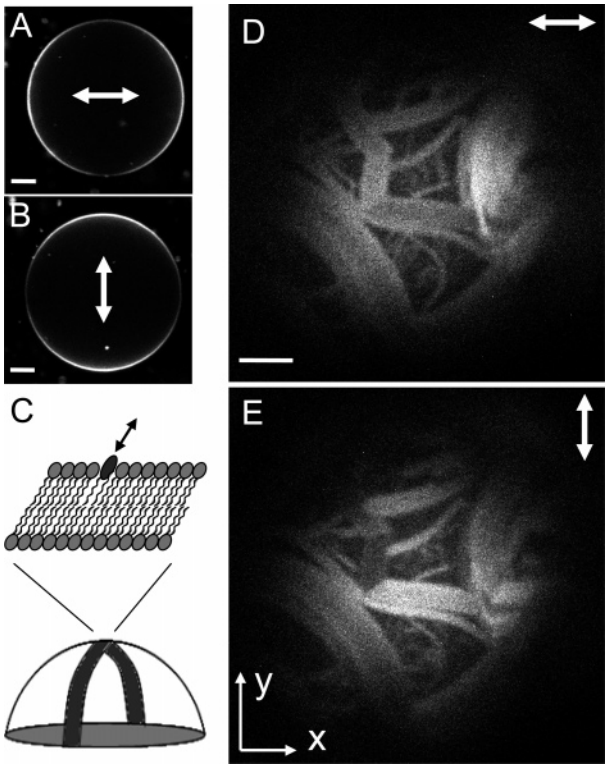

FIGURE 4: Characterization of lipid orientation by fluorescence polarization. (A, B) Confocal fluorescence images of a liquid-phase GUV composed of DLPC/DPPC (molar ratio 9:1) and labeled by 0.4% DiIC18. The laser beam is focused at the equatorial plane of the GUV. The excitation polarization is marked in the middle of the images. (C) Schematic of lipid orientation in a *y*-oriented stripe domain on the GUV top. The DiIC18 with its excitation dipole along the lipid chain is shown. The arrow represents the dipole direction of the probe in the bilayer. (D, E) Confocal fluorescence images of a GUV composed of DLPC/DPPC (molar ratio 1:9) and labeled by 0.4% DiIC18. The laser beam was focused at the GUV top. The excitation polarization is marked at the right upper corner of the images. For stripe domains along the *y* direction, the *x*-polarization excitation (D) produced a stronger DiIC18 signal than the *y*-polarization excitation (E). Bar = 10 μm.

we find that the fluorescence intensity with *y*-polarized excitation (I_y) is smaller than that with *x*-polarized excitation (I_x) with a ratio of $I_y/I_x = 0.52$. This result demonstrates that the lipids in *y*-oriented stripe domains are tilted along the *x* direction as shown in Figure 4C. We obtained the same results with Rh-DPPE-labeled stripe domains in 1:9 DLPC/DPPC GUVs (data shown in Supporting Information, Figure S1).

Due to the exclusion of fluorescent probes from the patch domains, we analyze the properties of these domains by CARS microscopy which permits direct imaging of specific molecules based on molecular vibration (*18*). Deuterated lipids were used in order to spectrally separate different lipid molecules (*19*, *20*). The fully deuterated hydrocarbon chains create a CD_2 symmetric stretch vibration at 2080 cm^{-1}, well separated from the CH_2 symmetric stretch vibration at 2840 cm^{-1}. Unlike the fluorescent lipid probe used as a marker of domains, the deuterated lipids are directly used as a component of the bilayer for CARS imaging. Using forward-detected CARS signals, Potma and Xie have shown that the gel domain in DSPC-d_{70}/DOPC GUVs is enriched in DSPC-d_{70} (*19*). In our experiment, we have observed that, at the same molar ratios, DOPC/DPPC-d_{62} GUVs show the same

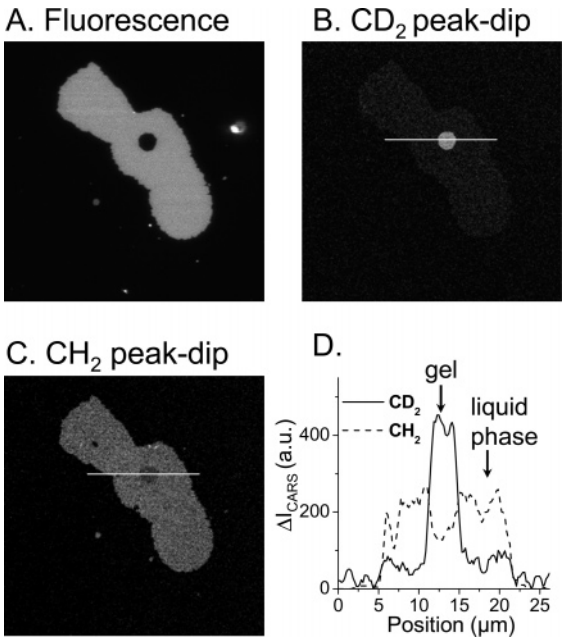

FIGURE 5: Characterization of patch domain composition by CARS microscopy. (A) Fluorescence image of a BODIPY PC labeled DOPC/DPPC-d_{62} (7:3) bilayer prepared by rupturing the GUVs onto a cleaned coverslip. The patch domain was not labeled by BODIPY PC and appeared dark in the middle of the bilayer. (B) E-CARS image of the same bilayer. The image was obtained by subtracting the E-CARS image taken at the dip of the CD_2 symmetric vibration (2125 cm^{-1}) from the E-CARS image taken at the peak position (2080 cm^{-1}). The wavelength of the pump beam was fixed at 709.8 nm. The pump and Stokes power at the sample were 3.0 and 1.4 mW, respectively, at a repetition rate of 3.8 MHz. (C) E-CARS image of the same sample obtained by subtracting the image taken at the dip of the CH_2 symmetric vibration (3000 cm^{-1}) from the image taken at the peak position (2840 cm^{-1}). (D) CARS intensity profiles along the lines shown in (B) and (C).

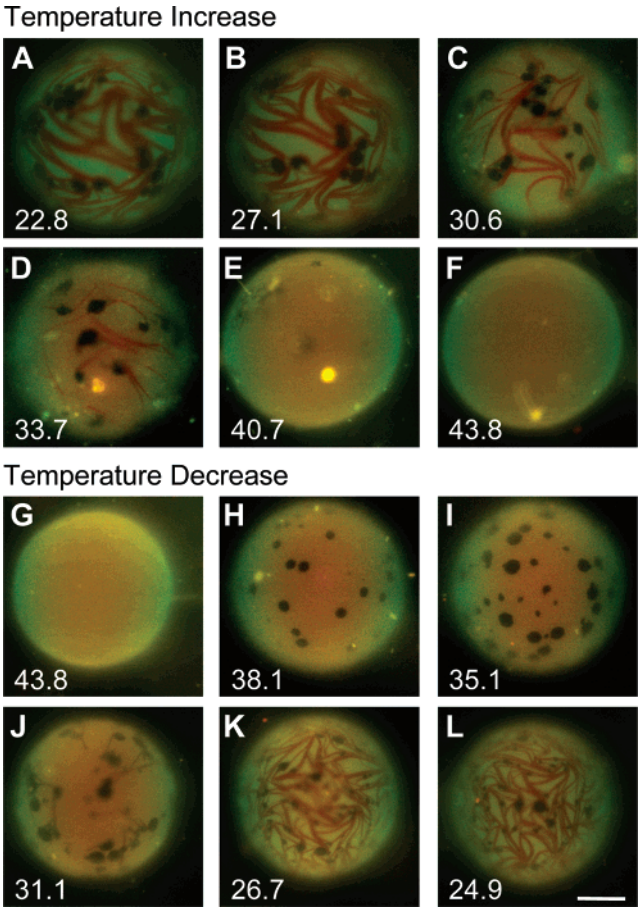

FIGURE 6: Fluorescence images of GUVs composed of DOPC/DPPC (molar ratio 2:8) acquired at different temperatures (°C) indicated in the images. The green and red pseudo colors represent the signal from BODIPY PC and Rh-DPPE, respectively. The confocal pinhole was not used in order to detect a larger area of the GUVs. Bar = 20 μm.

domain patterns as DOPC/DPPC GUVs (data not shown), indicating that deuteration induces little perturbation to phase segregation. We used epi-detected CARS (E-CARS) to avoid the large solvent background. To facilitate the E-CARS detection, we ruptured the GUVs onto a cleaned coverslip to form supported bilayers (*21*). The E-CARS signal is a coherent addition of the back-reflected CARS field from the water/glass interface and the CARS field from the bilayer (*20*, *22*). We note that the interaction between bilayer and coverslips might alter the lateral organization of lipids in bilayers. However, because GUV rupture was performed at room temperature, well below the domain melting temperature, we expect that, for the same sample, the lipid partition in the supported bilayer patch is close to that in the GUV bilayers.

Figure 5 shows the results for a bilayer composed of 7:3 DOPC/DPPC-d_{62} and 0.4% BODIPY PC. In the middle of the supported bilayer we observed a patch domain that is not labeled by BODIPY PC (Figure 5A). The patch domain produces a larger CARS signal in the difference image of the CD_2 vibration band (Figure 5B), while the BODIPY PC labeled liquid phase shows a stronger CARS intensity in the difference image of the CH_2 vibration band (Figure 5C). The difference of the CARS intensities measured at the peak and dip frequencies of a CARS band (ΔI_{CARS}) is proportional to the number of specific vibrational oscillators (e.g., the CD_2 groups) in the excitation volume (*20*). By comparing ΔI_{CARS} for the patch domain to that for the liquid phase (Figure 5D), we derive the partition ratio of DPPC-d_{62} between the patch domain and the liquid phase to be 5.7. The CARS intensity from CH_2 groups in the patch domain is 0.58 times that in the liquid phase. These results demonstrate that the patch domain is enriched in DPPC-d_{62} while the liquid phase is enriched in DOPC.

Lentz et al. have studied the phase diagram of DOPC/DPPC mixtures in both multilamellar liposomes and small unilamellar vesicles using fluorescence depolarization measurements (*23*). It was shown that DOPC and DPPC are not miscible at room temperature (*23*). As shown above, our imaging study has provided new details about the miscibility. To explore the thermodynamic properties of the stripe and patch domains, we have performed confocal fluorescence imaging of GUVs composed of 2:8 DOPC/DPPC in a temperature-controlled chamber. With increasing temperature the line width of the stripe domains became thinner, while the sizes of the patch domains did not change obviously (Figure 6B−D). The stripe domains finally melted into the liquid phase when further increasing the temperature to around 40 °C (Figure 6E). Interestingly, no transition from stripe to patch domains was observed. As the temperature reached 44 °C, both types of domains disappeared, resulting in a homogeneous distribution of Rh-DPPE and BODIPY PC in the GUV bilayer (Figure 6F).

After the GUV bilayer became homogeneous (Figure 6G), we cooled the same sample slowly to the room temperature. The patch domains appeared at 38 °C (Figure 6G). This temperature is between the DPPC pretransition (34 °C) and the main phase transition (42 °C) temperature (*24*). Further cooling the sample caused the growth of the patch domains in both size and number. When the temperature dropped to 31 °C, slightly below the DPPC pretransition temperature, we observed tiny Rh-DPPE-labeled stripe domains growing from the patch domains (Figure 6J). With continuing temperature decrease those lines became wider and more interconnected, eventually forming a network on the GUV surface (Figure 6K,L). Similarly, we did not observe any transition from patch domains to stripe domains, but the patch domains functioned as nucleation sites for the growth of stripe domains.

Using the micropipet aspiration technique (*13*, *25*, *26*), Needham et al. have shown that the membrane phase is correlated with the surface tension of vesicles (*14*). In our case, the surface tension of GUVs is induced by cooling. The cooling process following the electroformation not only causes a decrease of the GUV volume but also enhances the lipid−lipid interactions and induces a membrane tension. To find out whether the formation of stripe and patch domains depends on the GUV membrane tension, we varied the GUV surface tension and examined the domains formed after electroformation. We first used negatively charged lipids which were widely used to assist GUV formation in the gentle hydration method (*7*). The addition of negatively charged lipids introduces a long-range repulsive force inside the bilayer, which reduces the attractive interaction among phospholipids and lowers the surface tension accordingly (*27*). Adding 10% negatively charged DOPG into the 1:9, 2:8, and 3:7 DOPC/DPPC GUVs results in the disappearance of stripe domains and the formation of only patch domains (Figure 7A−C). Similar results were observed for GUVs made of 1:9, 2:8, and 3:7 DLPC/DPPC plus 10% DOPG (Figure 7D−F).

To release GUV surface tension without changing its composition, we prepared GUVs composed of 2:8, 3:7, and 4:6 DOPC/DPPC or DLPC/DPPC in sucrose solutions instead of Milli-Q water. Preparation of vesicles in a sucrose solution has been used to facilitate phase contrast imaging of GUVs (*25*). GUVs formed in a sucrose solution experience a smaller volume decrease than those formed in Milli-Q water because of the sucrose concentration gradient across the GUV membrane (*28*). As a result, the membrane surface tension is reduced. Using 10 and 100 mM sucrose solution, we did not see any obvious change of domain morphology compared to the GUVs formed in Milli-Q water (data not shown). However, when the sucrose concentration was increased to 1.0 M, we only observed patch domains at room temperature (Figure 7G−L), similar to the addition of 10% DOPG. In an alternative way, we prepared 2:8 DLPC/DPPC GUVs in 200 mM sucrose solution. The GUV solution was mixed with an equal amount of either 300 mM sucrose or 100 mM sucrose solution to reduce or enhance the membrane tension. The GUVs were then heated to 45 °C and cooled to room temperature. As a result, the use of 300 and 100 mM sucrose solutions led to the disappearance of stripe and patch domains, respectively (data shown in Supporting Information, Figure S2).

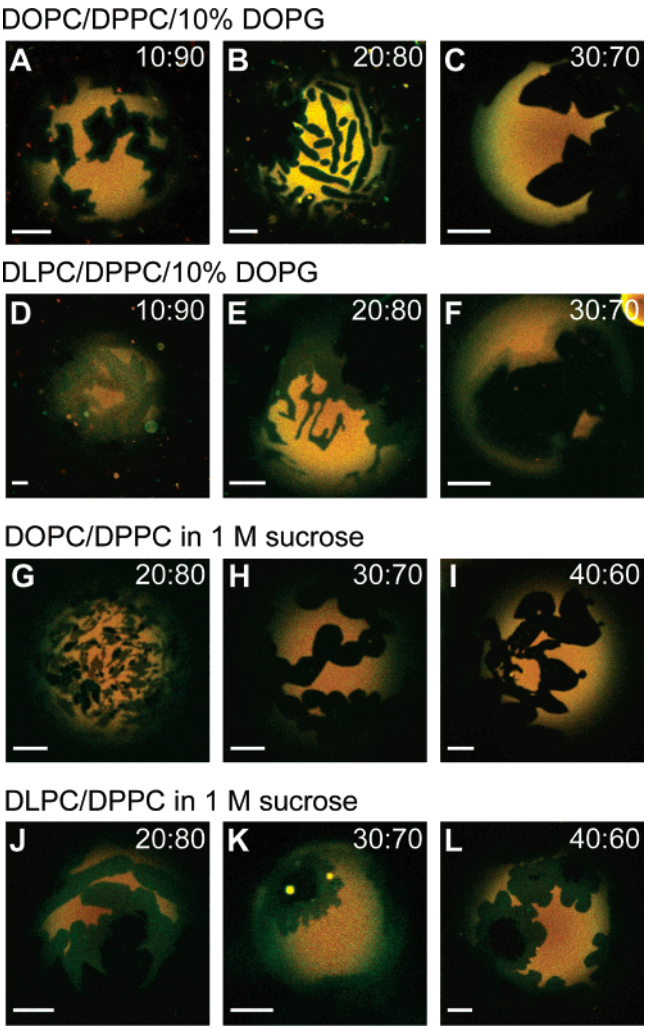

FIGURE 7: Release of surface tension leads to the disappearance of stripe domains visualized by confocal fluorescence microscopy. (A−C) Images of GUVs composed of DOPC/DPPC plus 10% DOPG. (D−F) Images of GUVS composed of DLPC/DPPC plus 10% DOPG. (G−I) Images of DOPC/DPPC GUVs prepared in 1.0 M sucrose solution. (J−L) Images of DLPC/DPPC GUVs prepared in 1.0 M sucrose solution. The molar ratio of DOPC:DPPC or DLPC:DPPC is marked in each image. Bar = 10 μm.

Interestingly, by adding 10% DOPG or carrying electroformation in 1.0 M sucrose solution, we extensively observed an interfacial domain between the patch domains and the liquid phase in the DLPC/DPPC GUVs (Figure 7). To analyze this new domain, we compared the fluorescence intensities of Rh-DPPE and BODIPY PC in different domains. The intensity profile along the white line in Figure 8A is shown in Figure 8B. The patch domain is not labeled by either probe. The liquid phase shows a strong fluorescence from Rh-DPPE and a relatively weak fluorescence from BODIPY PC, which we attribute to the fluorescence resonance energy transfer (FRET) between rhodamine and BODIPY. To verify the FRET effect in our samples, we prepared GUVs labeled by only BODIPY PC or Rh-DPPE. The interfacial domains were still observed (Figure 8C,D). Without Rh-DPPE, we observed a much stronger fluorescence from BODIPY PC in the liquid phase (Figure 8F). On the other hand, less fluorescent signal was probed from the liquid phase in GUVs labeled only by Rh-DPPE (Figure 8E). These results suggest a considerable FRET between Rh-DPPE and BODIPY PC in the liquid phase.

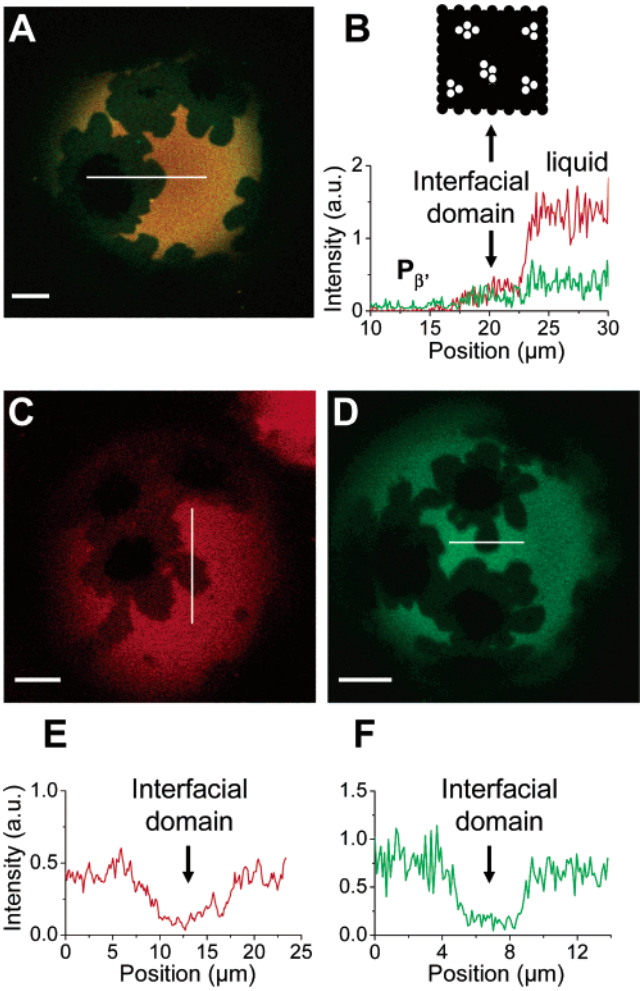

FIGURE 8: Confocal fluorescence image of the top of DLPC/DPPC GUVs (molar ratio 4:6) prepared in 1.0 M sucrose solution. (A) GUV labeled by 0.4% BODIPY PC and Rho-DPPE. (B) Intensity profile along the white line in (A). Red and green represent the intensities of Rh-DPPE and BODIPY PC, respectively. Shown above the intensity profiles is an illustration of molecular organization of the interfacial domain featured by nanoscale L_α domains in a continuous $P_{\beta'}$ phase. (C) GUV labeled by 0.4% Rho-DPPE only. (D) GUV labeled by 0.4% BODIPY PC only. (E, F) Fluorescence intensity profiles along the white line in (C) and (D). Bar = 10 μm.

DISCUSSION

We have presented a new phase behavior in GUVs composed of DOPC/DPPC and DLPC/DPPC. In both systems the patch-shaped domains appear at low DPPC fractions, while the stripe-shaped domains labeled by Rh-DPPE or DiIC18 show up at high DPPC fractions. Coexistence of both types of domains occurs at moderate DPPC fractions. Because DOPC and DLPC are different in acyl chain length and saturation, the same domain pattern observed in both binary lipid systems suggests that the domains are pertinent to the phase behavior of DPPC. It is established that DPPC bilayers undergo two thermal transitions above room temperature (*24*). One is a low-enthalpy pretransition and the other is a high-enthalpy chain melting transition (*29*). Below the pretransition temperature, DPPC forms a two-dimension lamellar structure in which the hydrocarbon chains are fully extended in an all-trans conformation and tilted with respect to the plane of the bilayer. This highly ordered structure is denoted as the $L_{\beta'}$ gel phase. The pretransition represents a transition from the $L_{\beta'}$ phase to a rippled structure denoted as the $P_{\beta'}$ phase which has been visualized in supported double bilayers with atomic force microscopy (*30*−*32*). We anticipate that the observed patch and stripe domains are correlated with the thermodynamic properties of DPPC, as discussed below.

The stripe domains can be preferentially labeled by Rh-DPPE or DiIC18. Both probes have been reported to favor the DPPC-rich phase over the coexisting fluid phase (*33*, *34*). Our systematic imaging study of DOPC/DPPC and DLPC/DPPC GUVs has shown that the line thickness of the stripe domains increases with increasing the molar percentage of DPPC (Figure 2). Moreover, the line thickness of the domains also relies on the temperature. With temperature increase, the stripe domains became thinner and eventually vanished (Figure 6). When cooling the GUVs from the miscibility temperature, the stripe domains appeared below the pretransition temperature of DPPC and became wider and more interconnected with further temperature decrease (Figure 6). Independent FCS studies by Scherfeld et al. (*12*) and Korlach et al. (*7*) have showed that stripe domains in DOPC/DPPC and DLPC/DPPC GUVs have a diffusion rate close to pure DPPC below the transition temperature (*35*). On the basis of these previous studies and our observations, we propose that the stripe domains are in the gel phase. This assignment agrees with a model proposed by Parasassi et al. that the network-shaped domains are like gel filaments into a liquid crystalline phase (*36*).

The stripe domains in GUVs were assigned as $P_{\beta'}$ or the nontilting L_β phase in different papers (*7*, *37*), but the lipid orientation has not been analyzed. Using polarized fluorescence microscopy (*17*, *38*), we have studied the long-range molecular orientation inside the stripe domains (Figure 4). We clearly observed that the fluorescence intensities from the stripe-shaped domains depended on the direction of the polarized excitation light. This implies that lipid chains in the stripe domains are tilted toward the boundary of the stripe domains as shown in Figure 4C. On the basis of the observed gel and anisotropic properties, we propose that the stripe domains are in the $L_{\beta'}$ phase. This assignment is consistent with the description that the $L_{\beta'}$ phase tends to arrange in a steplike structure which leads to a formation of a spiral shape (*39*).

Our CARS imaging study of the DPPC-d_{62}/DOPC-supported bilayer has shown that the patch domains are enriched in DPPC-d_{62} (Figure 5). Furthermore, we observed that the patch domains form below the miscibility temperature but above the pretransition temperature of DPPC (Figure 6). The enrichment in saturated lipids and the formation temperature suggest that the observed patch domains are in the $P_{\beta'}$ gel phase. This assignment is supported by the consistency in exclusion of any fluorescent probe by the patch domains in our GUVs and the $P_{\beta'}$ phase studied by Mesquita et al. (*40*).

The composition-dependent formation of patch and stripe domains in GUVs can be interpreted in the context of membrane mechanical properties. As shown by Needham and Evans (*14*), when cooling a fluid phase DMPC vesicle with the surface tension controlled by pipet suction, the $P_{\beta'}$ phase forms under zero or very low membrane stress, while the $L_{\beta'}$ phase forms under moderate membrane stress. In our case, the GUVs assume nearly zero surface tension at equilibrium state above the phase transition temperature of

DPPC (*41*). The cooling through the phase transition temperature not only shrinks the GUV diameter by approximately 7−8% but also increases the GUV volume to surface area ratio (*42*, *43*). This shrinkage of GUV volume strengthens the lipid−lipid interactions and builds up an excess surface tension accordingly (*26*). Because only the DPPC component in our GUVs experiences phase transition during the cooling process, the cooling-induced surface tension is higher with a larger molar fraction of DPPC. This relationship between the DPPC percentage and surface tension explains the domination of $L_{\beta'}$ stripe domains in GUVs containing a high DPPC molar fraction whereas only $P_{\beta'}$ patch domains appeared in GUVs containing a low DPPC molar fraction. The membrane tension theory also explains the broader existence range of $L_{\beta'}$ stripe domains in the DLPC/DPPC GUVs versus the DOPC/DPPC GUVs. Both acyl chains in DOPC are monounsaturated, generating a kink in the lipid chains. This may lower the hydrophobic interaction among lipids (*44*) and reduce the accumulation of surface tension in the GUV membranes, thus favoring the formation of $P_{\beta'}$ domains in the DOPC/DPPC GUVs. The same concept could also explain the change of domains upon temperature increase (Figure 6). During the initial stage of heating, the surface tension was high enough so that the $P_{\beta'}$ patch domains could not form during the melting of the $L_{\beta'}$ stripe domains. The direct transition from the $L_{\beta'}$ to L_α phase was previously observed in GUVs under external stress (*14*).

To further confirm that the observed domain pattern is tension dependent, we adopted two ways to reduce the surface tension of GUVs. The first way is to add negatively charged lipids into the GUV composition. Adding negatively charged lipids introduces a repulsive interaction which reduces the surface tension. As a result, the addition of 10 mol % DOPG eliminated the stripe domains in both DOPC/DPPC and DLPC/DPPC GUVs containing a high fraction of DPPC. The second way is to prepare GUVs in a high concentration sucrose solution. By this way we did not observe the stripe domains in GUVs containing a high fraction of DPPC. A quantitative analysis of the second method is presented below. The membrane tension is related to the osmotic pressure by the Laplace equation (*45*) $\Delta p = \{2\sigma\}/\{R\}$, where Δp is the Laplace pressure, σ is the surface tension, and R is the vesicle radius. The critical surface tension for GUVs is on the order of 1.0 mN/m (*41*). For a GUV with a radius of 20 μm, the critical surface tension corresponds to a normal pressure of 100 Pa based on the Laplace equation. Assuming a decrease of the GUV volume by 1% during the cooling process, a sucrose concentration difference of 0.01 M is created between the inside and the outside of a GUV formed in the 1.0 M sucrose solution. Because 1.0 M sucrose can produce an osmotic pressure as high as 20 atm (*45*), the 0.01 M sucrose concentration difference is able to generate a pressure of about 20000 Pa pointing toward the outside of the GUV. Under this condition the surface tension can be easily reduced to zero, leading to the formation of $P_{\beta'}$ instead of $L_{\beta'}$ domains in the GUVs. The reduced membrane tension also results in a decrease of line tension (*7*), which explains the change of the $P_{\beta'}$ domain shape in Figure 7 in comparison with Figures 2 and 3.

We would note that the $P_{\beta'}$ ripple phase with a stripe shape was observed in the supported double bilayer composed of 1:1 DMPC/DSPC by atomic force microscopy (*30*−*32*). Although this ripple phase is similar to our stripe domains in morphology, based on the following consideration, we would consider that the ripple phase in the supported double bilayers resembles the patch domains rather than the stripe domains we observed in GUVs. First, as shown in the literature (*46*, *47*), GUVs of the same lipid composition (1:1 DMPC/DSPC) exhibited patch domains but not stripe domains in the gel−fluid coexisting region. Second, after rupturing GUVs containing coexisting patch and stripe domains onto a supported DPPC bilayer (data shown in Supporting Information, Figure S3), we observed no stripe domains on the supported DPPC bilayer.

The difference between the stability of the ripple phase in supported double bilayers and that of patch domains in GUVs is discussed below. The $P_{\beta'}$ ripple phase in supported double bilayers only existed in a small temperature range (*31*). Decreasing temperature to below the pretransition temperature resulted in the dissipation of the $P_{\beta'}$ phase (*31*). However, the patch domains in GUVs are stable with temperature decrease and do not change into the stripe domains below the pretransition temperature of DPPC (Figure 6). This difference could be due to the interbilayer constraint existing in supported double bilayers. The bilayer−bilayer interactions may help to assist the flattening of the ripple phase with temperature decrease. In free-standing vesicles the transition from the rippled $P_{\beta'}$ phase to the planar $L_{\beta'}$ phase took hours to days as reported in previous SEM studies (*48*). External stress to the $P_{\beta'}$ phase vesicles was needed to increase the membrane stress and anneal the rippled membrane in a short time period (*14*). In general, the relationship between lipid domains in free-standing GUV bilayers and those in supported bilayers is an intriguing question. Our assignment of the patch and stripe domains is open to further analysis, for example, by examination of GUV domains by atomic force microscopy with new technical development.

By altering the surface tension by using DOPG or sucrose, we generated an interfacial domain between the patch domains and the liquid phase. The Rh-DPPE and BODIPY PC intensities from the interfacial domain are comparable (Figure 8B), indicating a lower FRET efficiency. Moreover, in GUVs labeled with only BODIPY PC, we observed much weaker fluorescence intensity from the interfacial domain than from the liquid phase (Figure 8F). On the basis of these results, we conceive that the interfacial domain is composed of a continuous $P_{\beta'}$ phase embedded with nanoscale L_α domains with size smaller than our spatial resolution of 250 nm (Figure 8B). This organization could explain the lowered FRET efficiency in the interfacial domain. In our sample, the FRET arises from the free motion of fluorescent probes. With the donors and acceptors partitioned into different nanoscale L_α domains, their total chance to encounter with each other is reduced (*49*, *50*). The formation of such nanoscale domains might result from reduction of the GUV surface tension and thus the line tension. We note that nanoscale domains were also reported in DLPC/DPPC GUVs containing a high fraction of cholesterol which reduces the membrane tension (*7*, *37*). The observed interfacial domains resemble the wetting layer formed in large unilamellar vesicles of $DC_{16}PC/DC_{22}PC$ to reduce the interfacial tension at the solid domain edge (*46*, *51*). Another possible organiza-

tion for the interfacial domain is decoupling of the two leaflets in the GUV bilayer. Indeed, such decoupling has been observed in supported bilayer (*52*, *53*) and small unilamellar vesicles with high curvature (*54*). However, the GUV bilayers are free standing with a low curvature, which does not favor the decoupling of the two leaflets.

CONCLUSIONS

We have identified a new phase segregation behavior, coexisting patch and stripe domains, in GUVs composed of DPPC/DOPC or DPPC/DLPC. The lipid molecules in the stripe domains are found to be tilted in a plane perpendicular to the stripe based on the DiIC18 fluorescence intensity dependence on the excitation polarization. CARS images reveal that the patch domains are enriched in DPPC-d_{62}. Temperature-controlled fluorescence imaging allowed us to visualize the formation process of these domains. The patch domains appear when the sample is cooled to between the chain melting and the pretransition temperature of DPPC. Cooling the sample to below the pretransition temperature causes the growth of stripe domains in GUVs containing a high molar fraction of DPPC. Heating the GUVs from room temperature causes the melting of stripe domains directly into the liquid phase. The stripe and patch domains are anticipated to be in the $L_{\beta'}$ and $P_{\beta'}$ gel phases, respectively. The observed $L_{\beta'}$ and $P_{\beta'}$ domains are interpreted as a result of composition-dependent GUV surface tension. The cooling generates a relatively larger surface tension in GUVs containing a higher molar percentage of DPPC, causing the formation of $L_{\beta'}$ domains. GUVs containing a lower molar percentage of DPPC have a lower surface tension, and thus only the $P_{\beta'}$ domains are observed. Our explanation is confirmed by the disappearance of stripe domains upon release of the surface tension by adding charged lipid component or applying an osmotic pressure to GUVs.

ACKNOWLEDGMENT

We thank Prof. Igal Szleifer for helpful discussions.

SUPPORTING INFORMATION AVAILABLE

Three figures as described in the text. This material is available free of charge via the Internet at http://pubs.acs.org.

REFERENCES

1. Simons, K., and Ikonen, E. (1997) *Nature 387*, 569−572.
2. Brown, D. A., and London, E. (1998) *Annu. Rev. Cell Dev. Biol. 14*, 111−136.
3. Mukherjee, S., and Maxfield, F. R. (2000) *Traffic 1*, 203−211.
4. Ikonen, E. (2001) *Curr. Opin. Cell Biol. 13*, 470−477.
5. Edidin, M. (2003) *Annu. Rev. Biophys. Biomol. Struct. 32*, 257−283.
6. Prestegard, J. H., and O'Brien, M. P. (1987) *Annu. Rev. Phys. Chem. 38*, 383−411.
7. Korlach, J., Schwille, P., Webb, W. W., and Feigenson, G. W. (1999) *Proc. Natl. Acad. Sci. U.S.A. 96*, 8461−8466.
8. Bagatolli, L. A., and Gratton, E. (2000) *Biophys. J. 78*, 290−305.
9. Veatch, S. L., and Keller, S. L. (2003) *Biophys. J. 85*, 3074−3083.
10. Baumgart, T., Das, S., Webb, W. W., and Jenkins, J. T. (2005) *Biophys. J. 89*, 1067−1080.
11. Dimova, R., Pouligny, B., and Dietrich, C. (2000) *Biophys. J. 79*, 340−356.
12. Scherfeld, D., Kahya, N., and Schwille, P. (2003) *Biophys. J. 85*, 3758−3768.
13. Shoemaker, S. D., and Vanderlick, T. K. (2003) *Biophys. J. 84*, 998−1009.
14. Needham, D., and Evans, E. (1988) *Biochemistry 27*, 8261−8269.
15. Staneva, G., Seigneuret, M., Koumanov, K., Trugnan, G., and Angelova, M. I. (2005) *Chem. Phys. Lipids 136*, 55−66.
16. Wang, H., Fu, Y., Zickmund, P., Shi, R., and Cheng, J. X. (2005) *Biophys. J. 89*, 581−591.
17. Moy, V. T., Keller, D. J., Gaub, H. E., and McConnell, H. M. (1986) *J. Phys. Chem. 90*, 3198−3202.
18. Cheng, J. X., and Xie, X. S. (2004) *J. Phys. Chem. B 108*, 827−840.
19. Potma, E. O., and Xie, X. S. (2005) *ChemPhysChem 6*, 77−79.
20. Li, L., Wang, H., and Cheng, J. X. (2005) *Biophys. J. 89*, 3480−3490.
21. Kaizuka, Y., and Groves, J. T. (2004) *Biophys. J. 86*, 905−912.
22. Potma, E. O., and Xie, X. S. (2003) *J. Raman Spectrosc. 34*, 642−650.
23. Lentz, B. R., Barenholz, Y., and Thompson, T. E. (1976) *Biochemistry 15*, 4529−4537.
24. Sackmann, E. (1995) in *Handbook of Biological Physics* (Lipowsky, R., and Sackmann, E., Eds.) pp 213−304, Elsevier, New York.
25. Rawicz, W., Olbrich, K. C., McIntosh, T., Needham, D., and Evans, E. (2000) *Biophys. J. 79*, 328−339.
26. Kwok, R., and Evans, E. (1981) *Biophys. J. 35*, 637−652.
27. Shoemaker, S. D., and Vanderlick, T. K. (2002) *Biophys. J. 83*, 2007−2014.
28. Evans, E., and Kwok, R. (1982) *Biochemistry 21*, 4874−4879.
29. Janiak, M. J., Small, D. M., and Shipley, G. G. (1979) *J. Biol. Chem. 254*, 6068−6078.
30. Leidy, C., Kaasgaard, T., Crowe, J. H., Mouritsen, O. G., and Jørgensen, K. (2002) *Biophys. J. 83*, 2625−2633.
31. Kaasgaard, T., Leidy, C., Crowe, J. H., Mouritsen, O. G., and Jørgensen, K. (2003) *Biophys. J. 85*, 350−360.
32. Giocondi, M.-C., and Le Grimellec, C. (2004) *Biophys. J. 86*, 2218−2230.
33. Bagatolli, L., Gratton, E., Khan, T. K., and Chong, P. L.-G. (2000) *Biophys. J. 79*, 416−425.
34. Spink, C. H., Yeager, M. D., and Feigenson, G. W. (1990) *Biochim. Biophys. Acta 1023*, 25−33.
35. Fahey, P. F., and Webb, W. W. (1978) *Biochemistry 17*, 3046−3053.
36. Parasassi, T., Krasnowska, E., Bagatolli, L. A., and Gratton, E. (1993) *Photochem. Photobiol. 57*, 403−410.
37. Feigenson, G. W., and Buboltz, J. T. (2001) *Biophys. J. 80*, 2775−2788.
38. Moy, V. T., Keller, D. J., and McConnell, H. M. (1988) *J. Phys. Chem. 92*, 5233−5238.
39. Krbecek, R., Gebhardt, C., Gruler, H., and Sackmann, E. (1979) *Biochim. Biophys. Acta 554*, 1−22.
40. Mesquita, R. M. R. S., Melo, E., Thompson, T. E., and Vaz, W. L. C. (2000) *Biophys. J. 78*, 3019−3025.
41. Sandre, O., Moreaux, L., and Brochard-Wyart, F. (1999) *Proc. Natl. Acad. Sci. U.S.A. 96*, 10591−10596.
42. Bagatolli, L. A., and Gratton, E. (1999) *Biophys. J. 77*, 2090−2101.
43. Kas, J., and Sackmann, E. (1991) *Biophys. J. 60*, 825−844.
44. Murzyn, K., Rog, T., Jezierski, G., Takaoka, Y., and Pasenkiewicz-Gierula, M. (2001) *Biophys. J. 81*, 170−183.
45. Levin, Y., and Idiart, M. A. (2004) *Phys. A 331*, 571−578.
46. Bagatolli, L. A., and Gratton, E. (2000) *Biophys. J. 79*, 434−447.
47. Fahsel, S., Pospiech, E.-M., Zein, M., Hazlet, T. L., Gratton, E., and Winter, R. (2002) *Biophys. J. 83*, 334−344.
48. Rüppel, D., and Sackmann, E. (1983) *J. Phys. 44*.
49. Loura, L. M. S., Fedorov, A., and Prieto, M. (2000) *Biochim. Biophys. Acta 1467*, 101−112.
50. Piknova, B., Marsh, D., and Thompson, T. (1996) *Biophys. J. 71*, 892−897.
51. de Almeida, R. F. M., Loura, L. M. S., Fedorov, A., and Prieto, M. (2002) *Biophys. J. 82*, 823−834.
52. Feng, Z. V., Spurlin, T. A., and Gewirth, A. A. (2005) *Biophys. J. 88*, 2154−2164.
53. Lin, W.-C., Blanchette, C. D., Ratto, T. V., and Longo, M. L. (2006) *Biophys. J. 90*, 228−237.
54. Almeida, P. F. F., Vaz, W. L. C., and Thompson, T. E. (1992) *Biochemistry 31*, 7198−7210.

BI060808H